Original

Aquila, A.; Sobierajski, R.; Ozkan, C.; Hajkova, V.; Burian, T.; Chalupsky, J.; Juha, L.; Stoermer, M.; Bajt, S.; Klepka, M.T.; Dluzewski, P.; Morawiec, K.; Ohashi, H.; Koyama, T.; Tono, K.; Inubushi, Y.; Yabashi, M.; Sinn, H.; Tschentscher, T.; Mancuso, A.P.; Gaudin, J.:

Fluence thresholds for grazing incidence hard x-ray mirrors

In: Applied Physics Letters (2015) AIP

DOI: 10.1063/1.4922380

Fluence thresholds for grazing incidence hard x-ray mirrors

A. Aquila,[1,a)] R. Sobierajski,[2] C. Ozkan,[1,b)] V. Hájková,[3] T. Burian,[3] J. Chalupský,[3] L. Juha,[3] M. Störmer,[4] S. Bajt,[5] M. T. Klepka,[2] P. Dłużewski,[2] K. Morawiec,[2] H. Ohashi,[6,7] T. Koyama,[6,7] K. Tono,[6,7] Y. Inubushi,[6] M. Yabashi,[6] H. Sinn,[1] T. Tschentscher,[1] A. P. Mancuso,[1] and J. Gaudin[1,c)]

[1]*European XFEL GmbH, Albert-Einstein-Ring 19, Hamburg D-22671, Germany*
[2]*Institute of Physics, PAS Al. Lotnikw 32/46, Warsaw PL-02-668, Poland*
[3]*Institute of Physics, ASCR, Na Slovance 2, CZ 182 21 Prague 8, Czech Republic*
[4]*Helmholtz-Zentrum Geesthacht, Max-Planck-Straße 1, Geesthacht D-21502, Germany*
[5]*Deutsches Elektronen-Synchrotron, Notkestraße 85, Hamburg D-22607, Germany*
[6]*RIKEN/SPring-8 Kouto 1-1-1, Sayo, Hyogo 679-5148, Japan*
[7]*Japan Synchrotron Radiation Research Institute (JASRI), Kouto 1-1-1, Sayo, Hyogo 679-5198, Japan*

(Received 25 March 2015; accepted 31 May 2015; published online 17 June 2015)

X-ray Free Electron Lasers (XFELs) have the potential to contribute to many fields of science and to enable many new avenues of research, in large part due to their orders of magnitude higher peak brilliance than existing and future synchrotrons. To best exploit this peak brilliance, these XFEL beams need to be focused to appropriate spot sizes. However, the survivability of X-ray optical components in these intense, femtosecond radiation conditions is not guaranteed. As mirror optics are routinely used at XFEL facilities, a physical understanding of the interaction between intense X-ray pulses and grazing incidence X-ray optics is desirable. We conducted single shot damage threshold fluence measurements on grazing incidence X-ray optics, with coatings of ruthenium and boron carbide, at the SPring-8 Angstrom compact free electron laser facility using 7 and 12 keV photon energies. The damage threshold dose limits were found to be orders of magnitude higher than would naively be expected. The incorporation of energy transport and dissipation via keV level energetic photoelectrons accounts for the observed damage threshold. [http://dx.doi.org/10.1063/1.4922380]

As X-ray Free Electrons Lasers (XFELs) approach terawatt power levels, knowledge of the fluence limits of X-ray optical coatings becomes increasingly important. It is difficult to use intense X-ray pulses without optics that can withstand the full intensity of the XFEL beam. All materials in the X-ray regime have complex indices of refraction, with typically the real part of the index being less than one. This means at very shallow angles, below a critical angle that is material and photon energy dependent, all materials have the property of total external reflection and are near perfect reflectors of X-rays. However, due to the index of refraction being complex, and hence exhibiting absorption, no grazing incidence mirror, or mirror coating, has a perfect 100% reflectivity of the incidence photons below its critical angle, and will therefore also absorb a fraction of the incident energy. Additionally, as X-ray mirrors operate in total external reflection, the attenuation length of the X-rays into the mirror potentially drops to nanometer scales, increasing the volumetric dose the material receives at its surface.

In this study, we used focused pulses from the SPring-8 Angstrom Compact free electron LAser (SACLA) XFEL[1] facility to measure the damage thresholds of two materials used for X-ray mirror coatings: boron carbide (B_4C) and ruthenium.

Boron carbide was chosen as it is commonly used in existing hard X-ray XFEL grazing incidence optics. This is due to its good thermal properties, high melting point, low density, and use of only low atomic number elements.[2] These last two properties increase the attenuation length by spreading out any absorbed energy over a larger volume, as well as increase the reflectivity. This comes, however, at the cost of reducing the critical angle at which the mirror can operate (which for a mirror of finite length limits the mirror's aperture).

Ruthenium was chosen as it represents another class of hard X-ray coated grazing incidence optics, namely, those with higher density and high Z metallic coatings. These optical coatings are typically found in optics at synchrotrons but not at existing hard X-ray FELs. The increased electron density of ruthenium increases its critical angle and allows it to operate at higher grazing angles—hence potentially higher numerical apertures—than materials like boron carbide. However, this trade off comes at the cost of a reduced attenuation length and a higher absorption below the critical angle. For high Z metal coatings, such as Ru, to be used as viable optics at XFELs, it is critical to know their single shot damage threshold fluence limit, as well as to understand the physical damage mechanism to predict the behavior of other materials and combinations.

To determine the damage thresholds, we exposed Ru and B_4C coated super polished flat silicon mirror substrates to

[a)]Present address: Linac Coherent Light Source, SLAC National Accelerator Laboratory, 2575 Sand Hill Road, Menlo Park, California 94025, USA.
[b)]Present address: Paul Scherrer Institut, CH-5232 Villigen PSI, Switzerland.
[c)]Present address: CEntre Lasers Intenses et Applications, U. Bordeaux, 351 cours de la Libration, 33405 Talence, France.

focused XFEL radiation at the SACLA facility. Measurements were conducted using single shots of a micron focused X-ray beam with photon energies of 7 and 12 keV, pulse energies of up to 100 μJ delivered on the sample, and pulse durations of order 20 fs. The X-rays were focused using a pair of Kirkpatrick-Baez (KB) optics,[3] with a full width at half maximum (FWHM) focal spot size of 1.20 μm vertical by 0.95 μm horizontal.

The samples consisted of 50 nm of sputtered Ru and B_4C on super polished mirror flats. Sample densities and the thickness of the thin films were measured using Mo K-α radiation as shown in Figure 1. Surface roughness was also measured using atomic force microscopy. Based on the coating densities measured, the attenuation lengths were also estimated for both materials as shown in Figure 1 and Table I. Of particular note is the nanometer attenuation length below the critical angle.

These test optics were mounted at grazing incidence angles in the focused SACLA XFEL beam. The optics were mounted such that the linear polarized FEL X-rays were reflected in a P-polarized geometry. The incidence angles for Ru coated substrates were measured to be 4.5 and 3.0 mrad for 7 keV and 12 keV, respectively. For the B_4C coated substrates, the incidence angles of 4.0 and 2.5 mrad were used for the 7 keV and 12 keV data, respectively. The shallower angles used for the B_4C optic is due to their lower critical angle than the Ru coated optic. All grazing angles were measured to better than 50 μrad using a downstream camera in the reflective 2θ geometry at low fluence, and hence, all measurements were conducted in the total external reflection regime. To adjust the fluence of the SACLA XFEL, aluminum and silicon solid attenuators were inserted upstream of the KB focusing optics. In addition, the XFEL pulses jitter in both photon energy and pulse energy, and therefore, single-shot electron diagnostics and X-ray gas cell diagnostics were used to measure these quantities, respectively.[4] X-ray

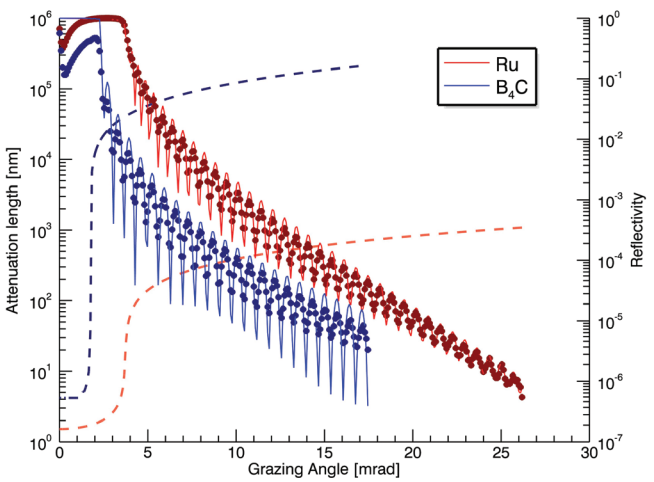

FIG. 1. Reflectivity measurements (circles) for Mo K-α radiation (17.5 keV) are shown for both B_4C (blue) and Ru (red) coated substrates. Density, thickness, and roughness have been obtained from fitting the reflectivity curves (solid lines). Using the density fitting parameter, modeling of the attenuation length into the material, as a function of grazing angle, is also shown (dashed lines). Below the critical angles of 1.75 and 3.77 mrad for B_4C and Ru, respectively, the attenuation lengths reach single nanometer values.

induced damage was observable for all samples below the critical angle with the exception of B_4C at 12 keV, where no physical damage to the mirror surface was detectable, even when the maximum available pulse energy was focused onto the sample.

Confocal microscopy was used to measure the lengths of the damaged surface induced by the single shot X-ray pulses as shown in Figure 2 for Ru and Figure 3 for B_4C. Additional image analysis was conducted using scanning electron microscopy and cross-sectioned transmission electron microscopy techniques on selected craters as shown for Ru in Figure 2 and for B_4C in Figure 3. Interestingly, the widths of the craters were often not continuous or uniform. For fluence threshold measurements, knowledge of the damaged area is required.[5] Estimates of the crater width were made by measuring the lengths of the damaged surface and then scaling by the incidence angle, as the transverse/perpendicular sizes of the FWHM focal spot size taken at normal incidence are nearly symmetric in both transverse directions. Standard methods were used to determine the fluence thresholds for damage[6–8] for the samples, as shown in Figure 4 and Table I. In the case of B_4C at 12 keV, only a lower bound could be given due to the lack of visible damage. We also note that the estimated beam size and shape were consistent with those determined by normal incidence measurements taken on lead(II) iodide[9] and on silicon oxide.[10]

It is of note that the fluence damage thresholds are far higher than the values obtained for normal incidence measurements or measurements conducted at lower photon energies.[11,12] This is due to a significant fraction of the pulse energy being reflected by the mirror coatings and not absorbed into the material. Additionally, the grazing angle increases the footprint of the XFEL beam reducing the effective fluence as compared to normal incidence. However, even if these two effects are taken into account, high values of the damage fluence are observed. It is noted that multi-shot damage measurements[13] on a similar system have observed an order of magnitude reduction in damage fluence compared to this work. The reduction is consistent with measurements conducted at soft X-rays where the single shot damage threshold is an order of magnitude higher than the observed multi-shot damage threshold.[12] This is potentially due to a related, but different, optical damage mechanism, such as carbon contamination of the optical surface.[14]

A rough estimate of the dose required to damage a material is to absorb enough energy to raise the material's temperature from room temperature to its melting point.[15] For ruthenium, this absorbed energy dose is 1.01 eV/atom[16] and for B_4C this dose threshold is 3.7 eV/atom.[17] However, as X-ray optic coating are thin films, care must be given to investigate and understand the interfaces between the film and the substrate.[18,19] For example, layers of B_4C and Si in B_4C/Si multilayers interdiffuse and form rough interfaces at temperatures of 300 °C,[20] which is far below the melting temperature of 2763 °C.

Using the measured damage threshold pulse energy, X-ray beam footprint area, and the $1/e$ extinction length to calculate the absorbed dose, one obtains a result that is >20 eV/atom absorbed threshold dose for B_4C, and well over 100 eV/atom for Ru. These values are unrealistic, since even

TABLE I. This table shows both experimental parameters used, as well as calculated values for each coating and photon energy explored. For the threshold fluence, the lateral size of the XFEL was taken into account. Note that the threshold fluence could not be calculated for B_4C at 12 keV, as the sample showed no visible signs of damage. In addition, as a significant fraction of the pulse energy is transmitted into the substrate, no realistic values of the damage dose could be calculated as they would relate more to the Si substrate than to the B_4C layer.

Material	Photon energy (keV)	Reflectivity (%)	Grazing angle (mrad)	$1/e$ X-ray extinction depth (nm)	Threshold fluence (J/cm^2)	Fraction of energy emitted as photoelectrons (%)	Calculated damage dose (eV/atom)
Ru	7	89.9	4.5	1.8	310	68	1.7
Ru	12	95.0	3.0	1.9	4700	67	0.98
B_4C	7	99.1	4.0	11.1	2400	55	…
B_4C	12	97.5	2.0	4.9	>10 000	55	…

non-thermal high excitation processes, like plasma formation, would occur at much smaller dose levels. As the materials show no visible signs of damage at fluence levels where the calculated dose far exceeds the expected damage threshold, a method of energy transport that distributes the absorbed energy over a larger volume could explain the observations shown in this work.

It has been proposed[21] that the energetic photoelectrons produced by the absorbed X-rays, with keV levels of kinetic energy, would ballistically transport the absorbed energy over a significantly larger volume and into the surrounding material. This would be conducted via multiple electron scattering events, as well as produce significant levels of photoelectrons escaping the surface to carry away the absorbed energy. These scattering events will cause secondary electron cascades as the energy is dissipated. To quantify this effect and model these processes, the PENELOPE[22,23] Monte Carlo simulation software package for electron/photon transport was used. The modeling begins by simulating photoelectrons produced at the surface of the modeled sample. The modeled sample consisted of 50 nm of the coating material (Ru or B_4C), followed by a thick Si substrate. As the dominant photoelectrons in B_4C come from the K shell, the simulations consisted of photoelectrons with momentum directions perpendicular to the surface following the electric field vector for the P-Polarization geometry. For the Ru simulations, the photoelectrons are split between the L_1 and $L_{2,3}$ shells. Therefore, simulations were conducted for photoelectrons produced both perpendicular to the surface, as well as photoelectrons distributed over 4π. This is to simulate the photoelectrons from the different shells. Auger electrons were not considered in the simulations as their kinetic energy is far lower than that of the photoelectrons. As the PENELOPE code models interaction event showers for one particle at a time and assumes the simulated material is static in state, processes caused by the intense femtosecond nature of the XFEL pulses, such as surface charging and photoelectron collision, are ignored in the modeling and place limits on the accuracy of the simulations. However, as we are trying to model the processes at energy densities just at

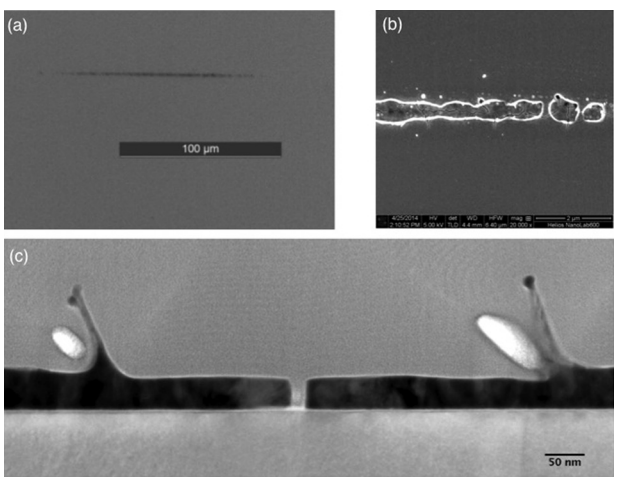

FIG. 2. (a) A typical confocal microscope image of a Ru damage crater at 7 keV used to determine the fluence thresholds. (b) A SEM of a damage crater for the Ru sample from a 12 keV X-ray pulse near the threshold fluence. Note that the crater is not continuous. (c) A cross-section TEM for the Ru sample from a 12 keV X-ray pulse. Note that Pt (top material) was used as a coating material to preserve the material for thinning for use in the TEM. Voids in the Pt layer (white) can be seen where the Ru bends over itself at the walls of the crater. In the Ru layer (dark central material), between 10 to 20 nm of material has been removed in the formation of the damage crater when compared to the thickness outside the crater. Additionally, a thin crack has formed in the center of the crater extending to the Si substrate (light colored bottom material). The crack is a sign of thermal expansion and the missing material with high edges is typical of a melting process initiated just at or below the surface.

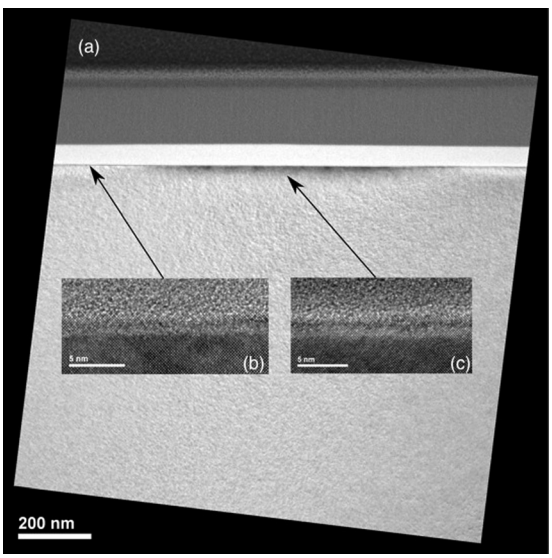

FIG. 3. (a) A cross-section TEM for the B_4C sample from a 7 keV X-ray pulse for a sample just above the damage threshold. Note that Pt (top material) was used as a coating material to preserve the sample for thinning for use in the TEM. The damage area is not a crater, as compared to the Ru in Figure 2, but a slightly raised bulge in the B_4C layer (white layer) is observed. The damage to the B_4C appears to be localized to the interface between the B4C and the Si substrate. The inset shows high resolution images of undamaged (b) and damaged (c) interfaces. In the high resolution damaged image, a slight expansion of the interface as the B_4C and the Si inter-diffuses is observed causing interface roughness.

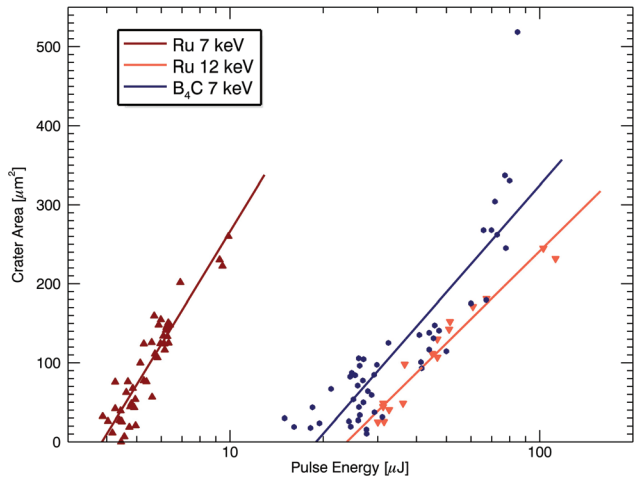

FIG. 4. Damage crater areas as a function of pulse energy are plotted on a log/lin scale for the B_4C and Ru coated substrates. Each data point is a single damage crater taken at different pulse energies, either due to inserted attenuators or the jitter of the XFEL. Exponential fits (solid lines) are used to determine the threshold fluence for each photon energy and coating material. The 12 keV B_4C coating data are not shown as no visible damage could be observed with the maximum 100 μJ pulse energies on sample obtainable at SACLA.

the onset of damage, where no plasma or non-linear effects are expected, the modeling is expected to give valid results.

One interesting result is that a significant fraction of the pulse energy is estimated to be emitted into the vacuum chamber as energetic photoelectrons. The estimated fraction of energy removed by photoelectrons escaping the sample is shown in Table I. For the energy that is absorbed into the mirror coating and the substrate, the simulated depth profile is shown in Figure 5. It is clear from Figure 5 that for B_4C, only a small fraction of the energy is actually absorbed in the B_4C layer. The significant fraction, >85%, of the absorbed energy is transmitted into the Si substrate; in addition, ~5% of the absorbed energy is absorbed at the B_4C/Si interface. It is hypothesized that this causes damage to the Si substrate at the interface just below the B_4C layer prior to the onset of damage to the optical coating. This is also indicated by the

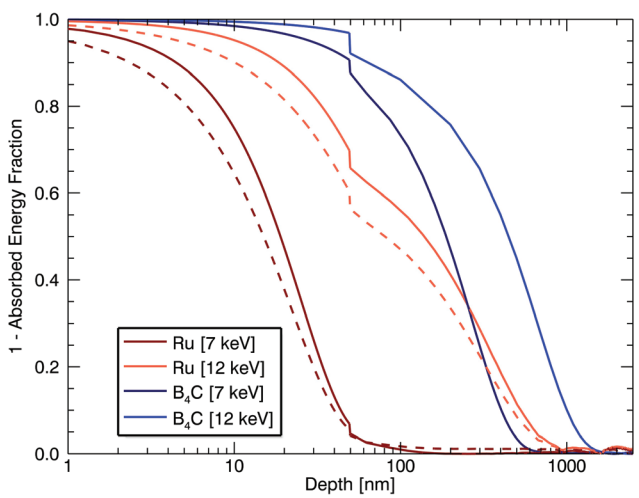

FIG. 5. PENELOPE simulations of the absorbed energy as a function of sample depth for B_4C and Ru. Note that the Si substrate begins at a depth of 50 nm. For the Ru data, the L_1 is in solid while the $L_{2,3}$ (electrons distributed over 4π) are shown as a dashed line.

cross-section TEM images shown in Figure 3. For the Ru coating, a significant fraction of the energy is absorbed in the Ru layer. Qualitatively, this is consistent with the cross-section TEM image in Figure 2, where the Ru layer shows signs of thermal damage such as cracking of the layer, and ablation of ruthenium. In all simulations, the deposition of the initial energy is dissipated into a volume one to two orders of magnitude larger than the $1/e$ X-ray attenuation length. Using the ballistic electron energy transport $1/e$ extinction depths obtained for Ru in the simulations (Figure 5), we obtain damage dose estimates (Table I) consistent with expected thermal damage estimates. For the B_4C damage, estimates cannot be given, as a significant fraction of the deposited energy is transported into the B_4C/Si interface and the Si substrate.

We have analyzed grazing incidence hard X-ray optical coating for damage caused by single intense XFEL pulses. We have determined the fluence levels that are sustainable for a low Z material (B_4C) and for a high Z metal coating (Ru). In both cases, the damage threshold is orders of magnitude higher than would be predicted by the energy density absorbed on the sample's surface. The calculated damage doses (Table I) are consistent with expected doses for thermal damage, when the transport of energy—via ballistic keV photoelectrons into a larger volume, and deeper into the sample, prior to the thermalization of these hot electrons with the optical coating and substrate—is included in the dose calculations.

Support from the operators of the SACLA facility is gratefully acknowledged. This work has been partially supported by the Polish National Science Center (Grant No. DEC-2011/03/B/ST3/02453), Academy of Sciences of the Czech Republic (M100101221) and the Czech Science Foundation (14-29772 S).

[1]T. Ishikawa, H. Aoyagi, T. Asaka, Y. Asano, N. Azumi, T. Bizen, H. Ego, K. Fukami, T. Fukui, Y. Furukawa *et al.*, Nat. Photonics **6**, 540 (2012).
[2]R. Soufli, M. Fernández-Perea, J. Krzywinski, D. W. Rich, S. L. Baker, J. C. Robinson, S. Hau-Riege, E. M. Gullikson, V. V. Yashchuk, W. R. McKinney *et al.*, Proc. SPIE **8777**, 877702 (2013).
[3]H. Yumoto, H. Mimura, T. Koyama, S. Matsuyama, K. Tono, T. Togashi, Y. Inubushi, T. Sato, T. Tanaka, T. Kimura *et al.*, Nat. Photonics **7**, 43 (2013).
[4]K. Tono, T. Togashi, Y. Inubushi, T. Sato, T. Katayama, K. Ogawa, H. Ohashi, H. Kimura, S. Takahashi, K. Takeshita *et al.*, New J. Phys. **15**, 083035 (2013).
[5]N. Gerasimova, S. Dziarzhytski, H. Weigelt, J. Chalupský, V. Hájková, L. Vyšín, and L. Juha, Rev. Sci. Instrum. **84**, 065104 (2013).
[6]J. M. Liu, Opt. Lett. **7**, 196 (1982).
[7]J. Chalupský, P. Boháček, V. Hájková, S. P. Hau-Riege, P. A. Heimann, L. Juha, J. Krzywinski, M. Messerschmidt, S. P. Moeller, B. Nagler *et al.*, Nucl. Instrum. Methods Phys. Res. A **631**, 130 (2011).
[8]A. Aquila, C. Ozkan, R. Sobierajski, V. Hájková, T. Burian, J. Chalupský, L. Juha, M. Störmer, H. Ohashi, T. Koyama *et al.*, Proc. SPIE **8777**, 87770H (2013).
[9]V. Hájková, L. Juha, P. Boháček, T. Burian, J. Chalupský, L. Vyšín, J. Gaudin, P. A. Heimann, S. P. Hau-Riege, M. Jurek *et al.*, Proc. SPIE **8077**, 807718 (2011).
[10]T. Koyama, H. Yumoto, Y. Senba, K. Tono, T. Sato, T. Togashi, Y. Inubushi, T. Katayama, J. Kim, S. Matsuyama *et al.*, Opt. Express **21**, 15382 (2013).
[11]J. Chalupský, V. Hájková, V. Altapova, T. Burian, A. J. Gleeson, L. Juha, M. Jurek, H. Sinn, M. Störmer, R. Sobierajski *et al.*, Appl. Phys. Lett. **95**, 031111 (2009).
[12]J. Krzywinski, D. Cocco, S. Moeller, and D. Ratner, Opt. Express **23**, 5397 (2015).

[13]T. Koyama, H. Yumoto, K. Tono, T. Sato, T. Togashi, Y. Inubushi, T. Katayama, J. Kim, S. Matsuyama, H. Mimura *et al.*, Proc. SPIE **8848**, 88480T (2013).
[14]R. Soufli, S. L. Baker, J. C. Robinson, E. M. Gullikson, T. J. McCarville, M. J. Pivovaroff, P. Stefan, S. P. Hau-Riege, and R. Bionta, Proc. SPIE **7361**, 73610U (2009).
[15]S. P. Hau-Riege, R. A. London, R. M. Bionta, M. A. McKernan, S. L. Baker, J. Krzywinski, R. Sobierajski, R. Nietubyc, J. B. Pelka, M. Jurek *et al.*, Appl. Phys. Lett. **90**, 173128 (2007).
[16]E. H. P. Cordfunke and R. J. M. Konings, Thermochim. Acta **139**, 99–106 (1989).
[17]M. W. Chase, Jr., "NIST-JANAF thermochemical tables, fourth edition," J. Phys. Chem. Ref. Data, Monogr. No. 9, 1–1951 (1998).
[18]Z. Jiang, X. Jiang, W. Liu, and Z. Wu, J. Appl. Phys. **65**, 196 (1989).
[19]R. Nüske, A. Jurgilaitis, H. Enquist, S. D. Farahani, J. Gaudin, L. Guerin, M. Harb, C. v. Korff Schmising, M. Störmer, M. Wulff, and J. Larsson, Appl. Phys. Lett. **98**, 101909 (2011).
[20]D. L. Windt, S. Donguy, J. F. Seely, B. Kjornrattanawanich, E. M. Gullikson, C. C. Walton, L. Golub, and E. DeLuca, Proc. SPIE **5168**, 1–11 (2004).
[21]R. A. London, R. M. Bionta, R. O. Tatchyn, and S. Roesler, Proc. SPIE **4500**, 51 (2001).
[22]J. Sempau, E. Acosta, J. Baro, J. M. Fernández-Varea, and F. Salvat, Nucl. Instrum. Methods B **132**, 377 (1997).
[23]J. Sempau, J. M. Fernández-Varea, E. Acosta, and F. Salvat, Nucl. Instrum. Methods B **207**, 107 (2003).